REPORT DOCUMENTATION PAGE

Form Approved
OMB No. 0704-0188

1. REPORT DATE *(DD-MM-YYYY)*	**2. REPORT TYPE**	**3. DATES COVERED** *(From - To)*
13-06-2007	Technical Paper	

4. TITLE AND SUBTITLE

Start-Up Response of Fluid Film Lubricated Cryogenic Turbopumps (Preprint)

5a. CONTRACT NUMBER
FA9300-04-C-0016

5b. GRANT NUMBER

5c. PROGRAM ELEMENT NUMBER

6. AUTHOR(S)
Luis San Andrés (Texas A&M University)

5d. PROJECT NUMBER
502603BY

5e. TASK NUMBER

5f. WORK UNIT NUMBER

7. PERFORMING ORGANIZATION NAME(S) AND ADDRESS(ES)

Northrop Grumman Space & Mission Systems Corp.
Space Technology
One Space Park
Redondo Beach CA 90278

8. PERFORMING ORGANIZATION REPORT NUMBER

AFRL-PR-ED-TP-2007-332

9. SPONSORING / MONITORING AGENCY NAME(S) AND ADDRESS(ES)

Air Force Research Laboratory (AFMC)
AFRL/PRS
5 Pollux Drive
Edwards AFB CA 93524-70448

10. SPONSOR/MONITOR'S ACRONYM(S)

11. SPONSOR/MONITOR'S NUMBER(S)
AFRL-PR-ED-TP-2007-332

12. DISTRIBUTION / AVAILABILITY STATEMENT

Approved for public release; distribution unlimited (07224A)

13. SUPPLEMENTARY NOTES
For presentation at the 43rd AIAA/ASME/SAE/ASEE Joint Propulsion Conference, Cincinnati, OH, 8-11 July 2007.

14. ABSTRACT

Reusable primary power cryogenic turbopumps (TPs) implement externally pressurized fluid film bearings to support the expected large thrust and lateral radial loads. Compact - low count part TPs operate super critically at exceedingly high shaft speeds (180 krpm) and with large pressure differentials. Hybrid journal bearings (HJBs) enable smaller and lighter turbopumps through no bearing DN life limitation. The growth of an "all-fluid-film- bearing" technology for reusable and less costly (per launch) TPs demands the development of analytical models and design tools accompanied by the testing of components. The paper presents a computational model for the prediction of the start-up performance of a flexible rotor supported on hydrostatic radial bearings. The transient response of rotor-bearing systems is of importance to determine safe operation and reliable dynamic performance under extreme loading conditions. In the start-up operation of a cryogenic TP, the fluid supply and discharge pressures, as well as the radial loads acting on the bearings, depend on pump rotor speed. The designed aerodynamic performance of the whole turbopump determines the schedule of rotor speed ramp-up. The start-up event is quite short in nature, lasting a few seconds at most. The bearing reaction forces are calculated from the numerical solution of unsteady bulk-flow equations including fluid inertia, flow turbulence, variable fluid properties and thermal energy transport. The equations of motion for the rotor and the fluid film bearings are solved numerically with local linearization at each integration time step. Predictions for the transient start-up response of a test rotor supported on water hydrostatic bearings are presented. The numerical results evidence the effect of rotor mass on the rotordynamic stability of the rotor-bearing system.

15. SUBJECT TERMS

16. SECURITY CLASSIFICATION OF:			**17. LIMITATION OF ABSTRACT**	**18. NUMBER OF PAGES**	**19a. NAME OF RESPONSIBLE PERSON**
					Alan Sutton
a. REPORT	**b. ABSTRACT**	**c. THIS PAGE**	SAR	38	**19b. TELEPHONE NUMBER** *(include area code)*
Unclassified	**Unclassified**	**Unclassified**			N/A

Start-up Response of Fluid Film Lubricated Cryogenic Turbopumps (Preprint)

Luis San Andrés[1]
Mechanical Engineering Department,
Texas A&M University, College Station, TX 77843

Reusable primary power cryogenic turbopumps (TPs) implement externally pressurized fluid film bearings to support the expected large thrust and lateral radial loads. Compact - low count part TPs operate super critically at exceedingly high shaft speeds (180 krpm) and with large pressure differentials. Hybrid journal bearings (HJBs) enable smaller and lighter turbopumps through no bearing DN life limitation. The growth of an "all-fluid-film-bearing" technology for reusable and less costly (per launch) TPs demands the development of analytical models and design tools accompanied by the testing of components. The paper presents a computational model for the prediction of the start-up performance of a flexible rotor supported on hydrostatic radial bearings. The transient response of rotor-bearing systems is of importance to determine safe operation and reliable dynamic performance under extreme loading conditions. In the start-up operation of a cryogenic TP, the fluid supply and discharge pressures, as well as the radial loads acting on the bearings, depend on pump rotor speed. The designed aerodynamic performance of the whole turbopump determines the schedule of rotor speed ramp-up. The start-up event is quite short in nature, lasting a few seconds at most. The bearing reaction forces are calculated from the numerical solution of unsteady bulk-flow equations including fluid inertia, flow turbulence, variable fluid properties and thermal energy transport. The equations of motion for the rotor and the fluid film bearings are solved numerically with local linearization at each integration time step. Predictions for the transient start-up response of a test rotor supported on water hydrostatic bearings are presented. The numerical results evidence the effect of rotor mass on the rotordynamic stability of the rotor-bearing system.

Nomenclature

A_o	$= C_d \pi d_o^2/4$. Effective orifice area [m^2]
b	= Recess circumferential length [m]
c	= Radial clearance function [m]
C_p	= Fluid specific heat [J/kg · °K]
$C_{XX}, C_{XY}, C_{YX}, C_{YY}$	= Damping force coefficients [Ns/m]
C_d	= Orifice discharge coefficient
D	$= 2 \cdot R$. Bearing diameter [m]
d_o	= Orifice diameter [m]
$f_{J,B}$	$= a_M \left[1 + \left(c_M \frac{r_{J,B}}{H} + \frac{b_M}{R_{J,B}} \right)^{e_M} \right]$; $a_M = 0.001375$, $b_M = 500{,}000$; $c_M = 10{,}000$, $e_M = 1/3.00$
	Turbulent flow friction factors at journal and bearing surfaces
$X_{(t)}, Y_{(t)}$	= Journal center eccentricity components [m]
F_X, F_Y	= Bearing fluid film forces along $\{X,Y\}$ axes [N]
h	$= c + X_{(t)} \cos(\theta) + Y_{(t)} \sin(\theta)$. Film thickness [m]
h_R	= Recess depth [m]
h_B, h_S	= Heat convection coefficients [J/kg · °K]
$K_{XX}, K_{XY}, K_{YX}, K_{YY}$	= Bearing force stiffness coefficients [N/m]
L, l	= Bearing axial length, recess axial length [m]

[1] Mast-Childs Professor

$M_{XX}, M_{XY}, M_{YX}, M_{YY}$ = Bearing inertia force coefficients [kg]
P, P_R, P_s = Fluid pressure, recess pressure, supply pressure [N/m^2]
Q_B, Q_S = Heat flow into bearing and journal (shaft) surface [J/kg]
Re = $(\rho\Omega CR/\mu)_*$. Nominal circumferential flow Reynolds number
Re_J, Re_B = $(\rho/\mu)h\sqrt{[(V_x - \Omega R)^2 + V_z^2]}$; $(\rho/\mu)h\sqrt{[V_x^2 + V_z^2]}$
Flow Reynolds numbers relative to journal and bearing surfaces
r_J, r_B = Surface roughness depths at journal and bearing [m]
t = Time [s]
T, T_s = Temperature, supply temperature [°K]
V_x, V_z = Bulk-flow velocities in circumferential (x) and axial (z) directions [m/s]
V_R = Recess volume including supply line [m^3]
W_X, W_Y = External loads applied on journal [N]
α = Fluid swirl ratio at recess edges
β_P = $(1/\rho)(\partial\rho/\partial P)$. Liquid compressibility coefficient [m^2/N]
β_T = $-(1/\rho)(\partial\rho/\partial T)$. Liquid volumetric expansion coefficient [1/°K]
θ = x/R. Circumferential or angular coordinate.
$\kappa_z = \kappa_x$ = $\frac{1}{2}(\kappa_J + \kappa_B)$. Turbulence shear factors along axial and circumferential flow directions
κ_J, κ_B = $f_J \cdot Re_J$, $f_B \cdot Re_B$. Turbulent shear parameters at journal and bearing surfaces
ρ, μ = Fluid density [kg/m^3], viscosity [Ns/m^2]
ξ_{xu}, ξ_{xd} = Empirical recess-edge entrance loss coefficients in circumferential (upstream, downstream) direction
ξ_z = Empirical recess-edge entrance loss coefficients in axial direction
Ω, ω = Rotational speed of journal, excitation or whirl frequency [1/s]
Subscripts refer to:
x,z = In direction of local circumferential and axial coordinates in plane of bearing
o = Orifice
R, e = Bearing recesses and edges (entrance)
u, d = Upstream and downstream of recess
B, J = Refer to bearing and journal surfaces

I. Introduction

Hydrostatic bearings (HBs) derive their load capacity not from shear flow driven effects (hydrodynamic wedge and surface sliding) but rather from the combination of pressure versus flow resistance effects through a feed restrictor and within the bearing film lands. Hydrostatic bearings can support large loads without journal rotation and provide large (accurate and controllable) direct stiffness as well as damping coefficients. The hydrostatic stiffness is of unique importance for the centering of high-precision milling machines, gyroscopes, large arena movable seating areas, telescope bearings, and even cryogenic fluid turbo pumps for rocket engines.

The importance of hybrid (combination hydrostatic and hydrodynamic) journal and thrust bearings and damping seal bearings as radial support elements in cryogenic turbomachinery has steadily grown over the past few years[1-3]. Compact - low count part turbo pumps (TPs) operate sub critically at exceedingly high shaft speeds (180 krpm) with pressure differentials as large as 550 bar. Advanced primary power require of externally pressurized fluid film bearings to support the expected large thrust and lateral radial loads. Hybrid journal bearings (HJB)s enable smaller and lighter turbopumps through no bearing DN life limitation and sub critical rotor operation, i.e. at speeds below the first elastic mode of the rotor-bearing system. HJBs offer durability, low friction and wear, accuracy of positioning, and large direct stiffness and damping force coefficients. These features enable the design (and operation) of un-shrouded impellers with a significant increase in the turbopump mechanical efficiency. The growth of an "all-fluid-film- bearing" technology for advanced and less costly (per launch cost) turbopumps demands the development of analytical models and design tools, the testing of components, and the implementation of the technology.

Hydrostatic bearings require an external pressurized supply system and some type of flow restrictor. Also, under dynamic motions, hydrostatic bearings may display a pneumatic hammer effect due to fluid compressibility. However, and most importantly, the load and static stiffness of a hydrostatic bearing are independent of fluid viscosity; thus making this bearing type very attractive for cryogenic liquid turbopumps or low viscosity process fluid pump applications.

Note that for the cryogenic fluid application as well as others handling low viscosity liquids, the large surface speeds and the large pressure differential determine flow conditions with high levels of flow turbulence and fluid inertia effects. Flow turbulence increases the lubricant "effective" viscosity, thus enhancing the load capacity due to hydrodynamic effects and increasing the bearing energy dissipation characteristics, i.e. more damping[1,2]. Computational programs based on the Reynolds equation of classical lubrication, i.e. no fluid inertia, are ill-prepared to render adequate predictions of hybrid bearing performance, static and dynamic force coefficients.

The author has developed the most comprehensive computational analyses for prediction of process fluid hybrid bearings, radial and thrust. The analyses address to the most important theoretical and practical issues related to the operation and dynamic performance of cryogenic fluid film bearings, i.e. geometric configuration, operating conditions, flow turbulence, fluid inertia, realistic fluid properties, thermal effects, and two-phase flow phenomena. References 1, 2 and 4-12 detail the computational analyses along with measurements to validate and calibrate the predictive codes. San Andrés[13] presents a comprehensive review of the static and dynamic performance characteristics of annular pressure seals and hydrostatic bearings for process fluid high performance pumps. The major advantages and disadvantages of hydrostatic bearings are thoroughly discussed with emphasis on remedies or fixes to reduce or even eliminate the potential for hydrodynamic instability and pneumatic hammer instability in actual TP applications.

The objective of the present analysis is to advance a computational model for the prediction of the start-up (or shut down) performance of a rotor supported on hydrostatic bearings. In the start-up operation of a cryogenic turbopump, the fluid supply and discharge pressures, as well as the radial loads acting on the hydrostatic bearings, depend on the pump rotor speed. The schedule of rotor speed ramp-up is defined by the designed aerodynamic performance of the whole turbopump. The start-up event is quite short in nature, lasting a few seconds at most.

The transient response of rotor-bearing systems is of importance to determine safe operation and dynamic performance under extreme loading conditions. San Andrés[14] already advanced a simpler model for the transient response of a point-mass rotor supported in turbulent flow, externally pressurized fluid film bearings. The equations of motion are solved numerically with local linearization at each integration time step. The bearing reaction forces are calculated from the numerical solution of unsteady bulk-flow equations including fluid inertia, turbulence, variable fluid properties and thermal energy transport. Examples follow for the transient response of damper seals and hydrostatic bearings under a variety of external loads. The nonlinear model needs small time steps with large execution times. Note that the analysis in Ref. 14 is limited to predictions of transient response at a fixed rotor speed. Presently, this severe shortcoming is removed.

II. Unsteady bulk flow analysis of turbulent flow hydrostatic bearings

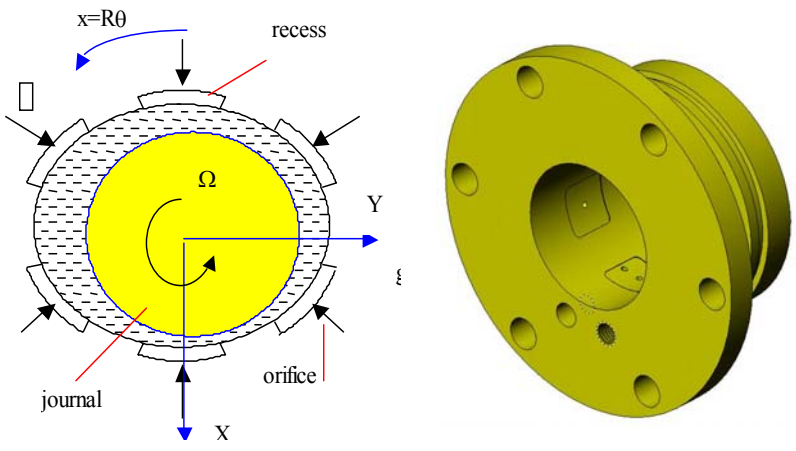

Figure 1. Schematic view of a radial hydrostatic/hydrodynamic journal bearing

Figure 1 shows the geometry of a hybrid (combination hydrostatic /hydrodynamic) journal bearing. A liquid at high pressure (P_s) is supplied through orifice restrictors and impinges into the bearing recesses with a mean pressure (P_R). The fluid injection is typically radial; though in some instances it could be at an angle opposing shaft rotation[2]. The pressure field within the recesses is determined from flow continuity with the film lands, momentum exchange at the orifice plane and a viscous rise due to journal rotation. At the recess edges, an inertial pressure drop also occurs due to the sudden transition from the recess of depth (h_R) into the film lands of thickness (h). Past the recesses, the liquid then flows through the film lands and the pressure

[2] Angled injection aids to reduce the development of circumferential flow speed and reduce, even eliminate, the magnitude of cross-coupled stiffness coefficients[11].

drops to the discharge value (P_a).

The computational model considers the fully developed turbulent bulk-flow of a fluid whose material properties depend on its local thermo physical state of pressure and temperature. That is, the fluid density (ρ), viscosity (μ) and heat capacity (C_P) are functions of the local pressure (P) and temperature (T). The fluid flows within the film lands of film thickness (h) with buk-flow (film averaged) circumferential and axial flow velocities denoted by V_x and V_z, respectively. The general bulk-flow transport equations are[1]:

$$\frac{\partial(\rho h\psi)}{\partial t}+\frac{\partial(\rho hV_x\psi)}{\partial x}+\frac{\partial(\rho hV_z\psi)}{\partial z}=S \tag{1}$$

where	Variable	Source term, S	
conservation of mass equation	$\psi = 1$	0	(2a)
transport of circumferential *(x)* momentum velocity	$\psi = V_x$	$-h\frac{\partial P}{\partial x}-\frac{\mu}{h}\left(\kappa_x V_x-\kappa_J\frac{\Omega R}{2}\right)$	(2b)
transport of axial momentum *(z)* velocity	$\psi = V_z$	$-h\frac{\partial P}{\partial z}-\frac{\mu}{h}(\kappa_z V_z)$	(2c)
transport of thermal energy	$\psi = C_p T$	$-Q_{BS}+\beta_T h T\left(\frac{\partial P}{\partial t}+V_z\frac{\partial P}{\partial z}+V_x\frac{\partial P}{\partial x}\right)+$ $R\Omega\cdot\tau_{y\theta}\Big\|^{h}+V_z\cdot\Delta\tau_{zy}+V_x\cdot\Delta\tau_{y\theta}$	(2d)

Above, $(\kappa_x\ \kappa_z)$ denote wall shear stress turbulent flow coefficients. The wall shear stress parameters $\kappa_z=\kappa_x=\frac{1}{2}(\kappa_J+\kappa_B)$ with $\kappa_J=f_J\ Re_J$, $\kappa B=f_B\ Re_B$, and the Moody's friction factors ($f_{J,B}$) depend on the bearing and journal surface conditions and the flow Reynolds numbers, Re_J and Re_B, relative to the rotating and stationary surfaces, respectively[15]. The bearing film thickness relates the rotor motion at the journal location to the bearing fluid flow,

$$h=c_{(x)}+X_{(t)}\cos(\theta)+Y_{(t)}\sin(\theta) \tag{3}$$

and its time derivative, dh/dt. Above, c is the bearing clearance at the journal centered position, and (X, Y) are the instantaneous journal center displacements. The journal eccentricity follows from $e=(X^2+Y^2)^{1/2}$. In the transport of thermal energy, Eq. (2d), $Q_{BS}=Q_B+Q_S=h_B\ (T-T_B)+h_S\ (T-T_S)$ is the heat flow through the bearing and shaft surfaces at temperatures T_B and T_S, respectively . β_T is the coefficient of thermal expansion, (h_B , h_S) are heat convection coefficients, and $\Delta\tau_{zy}$ and $\Delta\tau_{y\theta}$ are wall shear stress differences along the axial and circumferential directions, respectively.

In most time transient response analyses, the time scales for thermal energy transport and diffusion are much slower than those for mechanical energy (due to vibrations, for example). Hence a quasi-state energy transport is assumed, with the temperature remaining constant during a relatively fast transient process, i.e. $\partial T/\partial t\approx 0$.

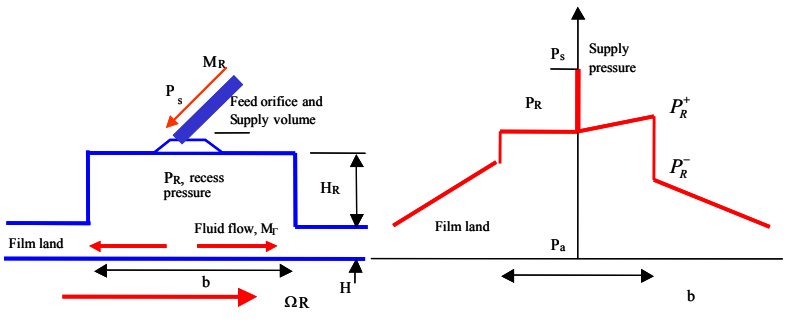

Figure 2. Schematic view of approximate pressure field in a pocket of a hydrostatic bearing

Figure 2 depicts a bearing recess with axial length (l) and circumferential extent (b). The recess area $A_R=l\ x\ b$, and the feed orifice has diameter d_o with feed volume V_{supply}. The simplified analysis of hydrostatic bearings does not model the flow field within the recess since these are (typically) deep and enclose a nearly stagnant fluid volume. The bulk-flow model accounts for mass flow continuity with the film lands and obtains the recess pressures (P_R) from

an orifice flow equation whose accuracy depends on an empirical discharge coefficient (C_d). CFD results and measurements show the generation of hydrodynamic pressures within the pocket, followed by sharp inertial pressure drops at the recess edges.

The continuity equation at a hydrostatic recess establishes a balance among the mass flow through the feed orifice (M_R), the flow through the boundaries of the recess into the film lands (M_Γ), and the accumulation of fluid mass within the recess volume, $V_R=[A_R\,(h+h_R)+V_{supply}]$. That is,

$$M_R = C_d\, A_o \left(\frac{\rho}{2}\left[P_s - P_R\right]\right)^{1/2} = M_\Gamma + \frac{\partial}{\partial t}\left(\rho V_R\right) \tag{4}$$

where $A_o = C_d(\pi d_o^2/4)$ is the effective orifice area, and $M_\Gamma = \oint_\Gamma \left(\rho h\, \vec{V}\cdot\vec{\eta}\right) d\Gamma$ is the outflow from the pocket into the bearing film lands. The circumferential pressure downstream of the feed orifice, P_R^+, increases as in a Rayleigh step bearing, i.e.

$$P_R^+ = P_R + \mu\kappa_x \frac{b}{2\left(h+h_R\right)^2}\left\{\frac{\Omega R}{2} - V_x\right\}_R \tag{5}$$

Fluid inertia causes a sudden pressure drop at the interface between a recess and the film lands. The fluid pressures, P_R^-, entering into the film lands bounding a recess are

$$P_R^- = P_R^+ + \frac{(1+\xi)}{2}\rho\left[1 - \left(\frac{\rho_e^-}{\rho_e^+}\right)\left(\frac{h}{h+h_R}\right)^2\right] V_{x,z}^2 \tag{6}$$

where (ξ) represents empirical entrance loss coefficients at the recess edges, axial and circumferential. The sudden pressure drop is accounted for only if the fluid flow effectively enters into the thin film lands.

Recall that severe subsynchronous vibrations at rotational speeds above a certain threshold denote a hydrodynamic instability on rotor-fluid film bearing systems and due to the effect of journal rotational speed on the shear flow field. This condition is typical of fixed geometry bearings. The threshold speed corresponds to the rotor speed at which a bearing is deprived from its effective damping and any small perturbation from an equilibrium position will determine unbounded rotor motions. The whirl frequency ratio (*WFR*) denotes the ratio between the onset whirl frequency (typically the system first critical speed) and the threshold speed of instability. Plain journal bearings show a *WFR* equal to 0.50 for small to moderate operating eccentricities (light loads), and thus instability onsets at rotational speeds equal to twice the system first critical speed. Measurements in hybrid bearings verify closely the prediction of *WFR* =0.50, see Ref. 10. In some circumstances the *WFR* even increases above 0.50, in particular for low rotational speeds and large supply pressures.

San Andrés and Childs[11] extend the bulk-flow model to account for fluid injection at an angle and opposing shaft rotation. This design feature retards the full development of the circumferential flow velocity, thus reducing the cross-coupled stiffness coefficients which prevent the operation of hybrid bearings at large rotational speeds.

III. Numerical solution of unsteady bulk-flow equations

In the numerical analysis, an implicit scheme is implemented on finite size control surfaces[16] with the *SIMPLEC* algorithm[17]. In general, the discrete algebraic equation for each variable $\varphi = \{V_x,\, V_z,\, P,\, T\}$, at the current time ($t$), is of the form

$$A_p^\phi \phi_p = A_E^\phi \phi_E + A_W^\phi \phi_W + A_S^\phi \phi_S + A_N^\phi \phi_N + S_p^\phi + B_p^\phi\, \phi_p^{(t-\Delta t)} \delta t \tag{7}$$

where $\phi_p^{(t-\Delta t)}$ is the value of the variable one time step before. That is, at each time step, the previous flow field must be known fully; in particular the one at the initial time when the solution procedure starts. San Andrés[18] details the development of the algebraic equations for momentum, mass and energy transport in thin film bulk-flows. Once the solution of the set of Eq. (7) is obtained at time t, fluid film bearing reaction forces (F_X, F_Y) are calculated from integration of the pressure field, i.e.

$$\begin{Bmatrix} F_X \\ F_Y \end{Bmatrix}_{(t)} = \int_0^L \int_0^{2\pi R} (P - P_a) \begin{bmatrix} \cos\theta \\ \sin\theta \end{bmatrix} R\, d\theta\, dz \tag{8}$$

The bearing reaction forces are also known as (nonlinear) impedances since they are a function of the instantaneous journal center position and its velocity components, i.e.

$$F_X = f_X\left(X, Y, \dot{X}, \dot{Y}\right);\ F_Y = f_Y\left(X, Y, \dot{X}, \dot{Y}\right) \tag{9}$$

A rotordynamics model predicting the transient response of a rotor supported on bearings needs to integrate the (nonlinear) bearing impedances at each time step. The typical equations of motion are of the form

$$[M]\{\ddot{u}\} - [[C] - \Omega[G]_R]\{\dot{u}\} + [K]\{u\} = \{F_{ext}(u, \dot{u}, t)\} + \{F_B(u, \dot{u})\} \tag{10}$$

where Ω is the rotor speed, and [*M*], [*K*], [*C*] and [G] denote the system mass, stiffness, damping and gyroscopic matrices. The vector $\{u\}$ represents rotor displacements (translations and rotations), $\{F_{ext}(u, \dot{u}, t)\}$ denotes external forces such as static (gravity) loads and those due to mass imbalance, and $\{F_B(u, \dot{u})\}$ corresponds to the nonlinear bearing impedances, for example, i.e. Eq. (8). Note that the solution of the rotor-bearing system equations of motion, Eq. (10), is linked to the solution of the bulk-flow equations for each bearing support, Eq. (7).

The interface of the current predictive hydrostatic bearing bulk-flow model to a comprehensive (realistic) rotordynamics model is being completed. At this time, for testing of the code features, a simple point mass rotor-bearing model suffices. The equations of motion for the simple system are

$$M\,\ddot{X} = W_X + F_X, \quad M\,\ddot{Y} = W_Y + F_Y \tag{11}$$

where *M* denotes the rotor mass, (W_X, W_Y) and (F_X, F_Y) are the components of the externally applied force and the bearing reaction forces, respectively.

The numerical solution of Eq. (11) implements the implicit Wilson-θ method as given by Bathe[19] and reproduced in Ref. 14 with θ=1.42. At each time step, Eq. (11) is an algebraic nonlinear equation whose unique solution is determined with the aid of linearized stiffness and damping coefficients.

IV. Predictions of transient speed response of a simple rotor supported on water lubricated hydrostatic bearings

A unique test rig has been constructed at Texas A&M University for purposes of recording the start up response of a rotor supported on a water lubricated hydrostatic bearing. The test apparatus will replicate a typical rotor speed start-up in a cryogenic TP and measure the operating conditions best suited for early rotor lift off. Shallow pockets of small area are preferred in high performance TPs to avoid pneumatic hammer effects when handling compressible liquids. Details of the specific bearing configuration are omitted for brevity. In the experiments, warm water will be supplied into the bearings with increasing supply pressures tied to the rotor speed ramp-up. For the current predictions, isothermal flow conditions prevail in the bearings since the flow rates are large and the shaft speed-up ramp is very fast. That is, in the analysis the fluid temperature remains at its inlet condition.

Figure 3 shows the schedule of a fast transient for the envisioned test rig. The figure displays the rotor speed, water supply pressure and external radial load acting on the bearing versus time. For times less than 0.015 sec, the rotor speed increases linearly with time from 5 krpm to 20 krpm. Over the same time interval, the radial load also increases linearly from 100 N to 300 N, while the supply pressure has a quadratic increase, i.e. proportional to rotor speed^2. For times larger than 0.015 sec, the speed, feed pressure and load remain invariant. Figure 4 depicts the feed pressure and radial load (W_X, W_Y=0) versus rotor speed. Over the time span from 0 s to 0.027 s, the total number of shaft revolutions is just seven.

In the transient rotor response (nonlinear) analysis, a time step Δt=33.3 micro-s is used, corresponding to a sampling rate of 30 kHz. For the lowest and top shaft speeds of 5 krpm and 20 krpm (83 Hz & 333 Hz), the number of steps per shaft revolution equals to 360 and 90, respectively. The fast speed ramp rate, 15 krpm/0.015 sec (16.6 kHz/sec) demands the very small time step for integration of Eq. (11).

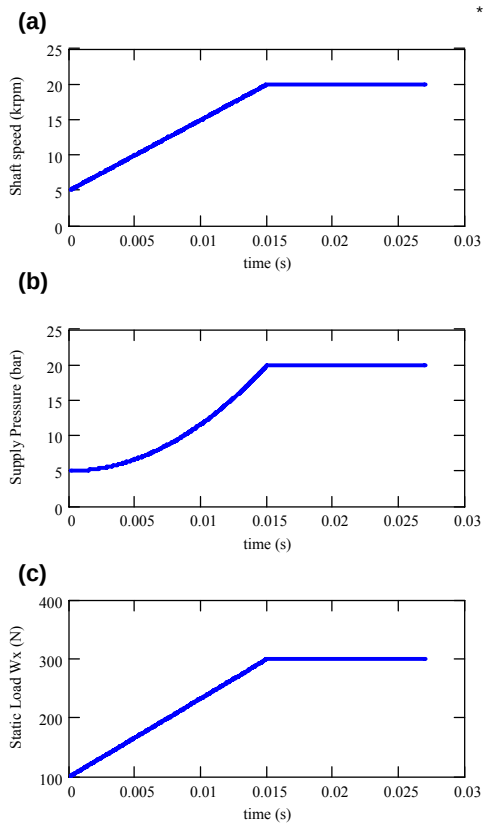

Figure 3. Example transient rotor speed, supply pressure and static load vs. time for water HB test rig

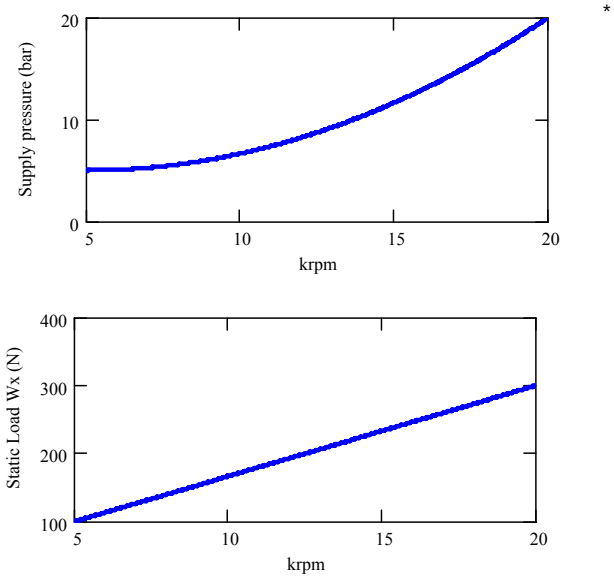

Figure 4: Example transient supply pressure and static load vs rotor speed for water HB test rig

Numerical predictions of hydrostatic bearing static performance were obtained prior to conducting the integration of the rotor-bearing system transient response during the ramp up in shaft speed. Table 1 depicts the values of speed, supply pressure and static load acting on the bearing, and the predicted rotor static position (X_S, Y_S) mass flow and power loss, equivalent stiffness, whirl frequency ratio and critical mass at the noted shaft speeds. Note that the whirl frequency ratio (*WFR*) is $>\sim 0.50$ for all speeds, denoting the potential of the bearings to induce a hydrodynamic instability. The critical mass parameter decreases rapidly as the rotor speed increases. The threshold speeds of instability are also noted for two rotor masses (M) equal to 1 and 10 kg. For the largest rotor mass, a threshold speed of 20.36 krpm is very close to the top shaft speed (20 krpm)[3].

As an initial condition for the numerical integration of the equations of motion, the flow field corresponding to the journal static position at the lowest shaft speed (5 krpm) was used, i.e. X/c=0.38, Y/c=0.15. Figures 5and 6 depict the predicted dimensionless (with respect to bearing clearance) journal eccentricity and its components (X,Y) versus shaft speed and versus time, respectively. The graphs include the results for rotor mass equal to 1 kg and 10 kg. For the smallest rotor mass, M=1 kg, the dynamic response predictions agree well with the static load calculations; and most importantly show a stable rotor-bearing system. On the other hand, for the largest rotor mass, M=10 kg, the transient response quickly evolves into an oscillatory pattern with increasing amplitudes of motion, typical of the onset of a hydrodynamic instability. The frequency of whirl is subsynchronous, tracking the rotor speed at roughly 55% WFR.

[3] The predictions for critical mass and threshold speed of instability do account for fluid inertia effects in the bearings. This effect amounts to 27% of the static direct stiffness at the top shaft speed.

(a) rotor mass, *M*=1 kg

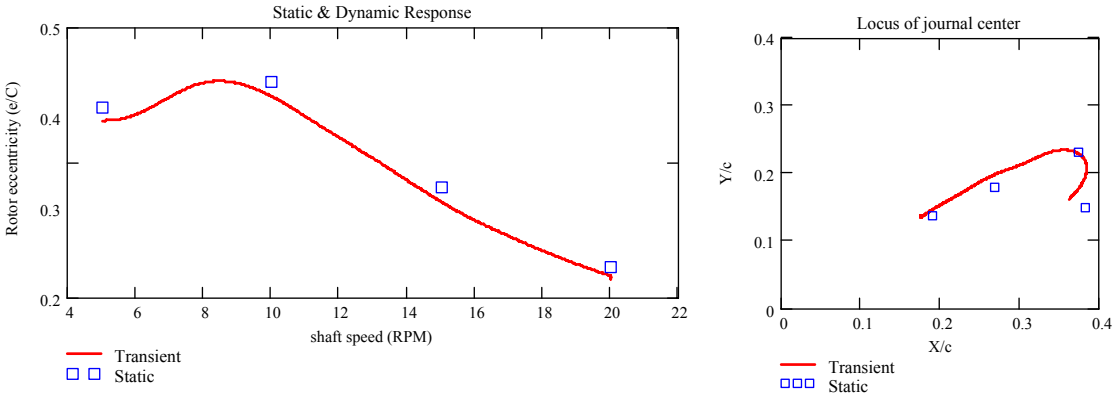

(b) rotor mass, *M*=10 kg

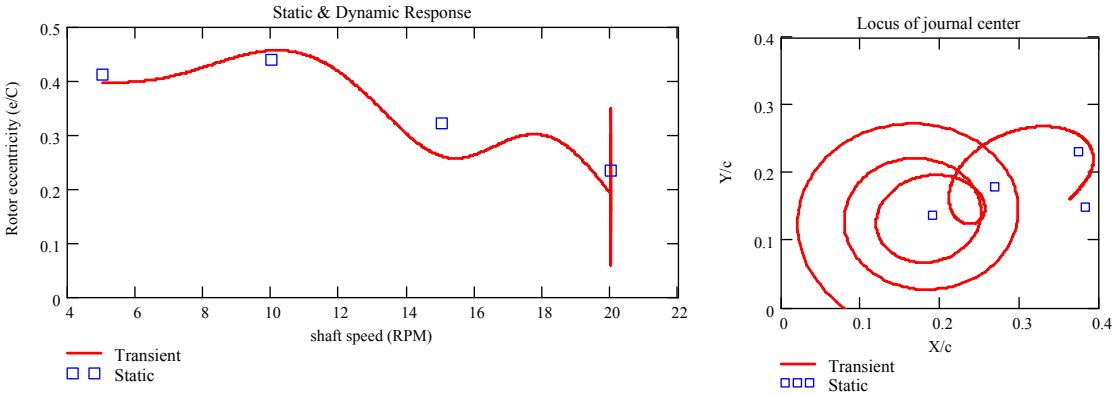

Figure 5. Predicted dimensionless journal (rotor) eccentricity versus shaft speed (a) M=1 kg, (b) M=10 kg. Static load journal eccentricity shown as square symbol.

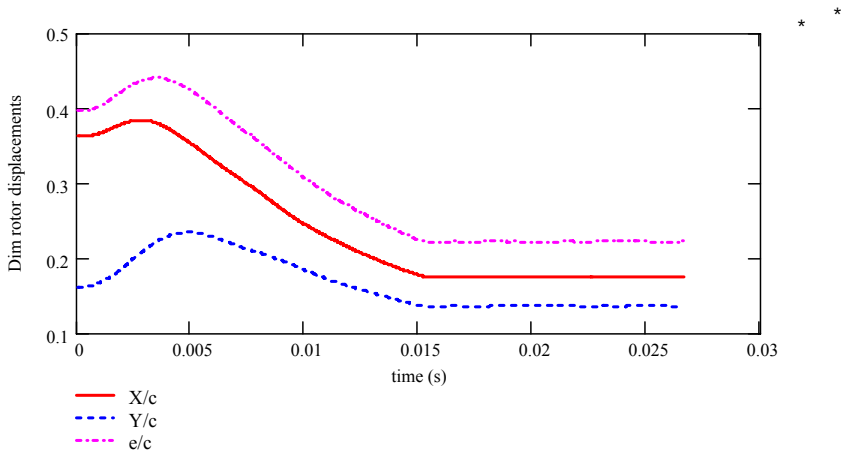

Figure 6a: Predicted dimensionless journal (rotor) eccentricity components versus time. Rotor mass *M*=1 kg

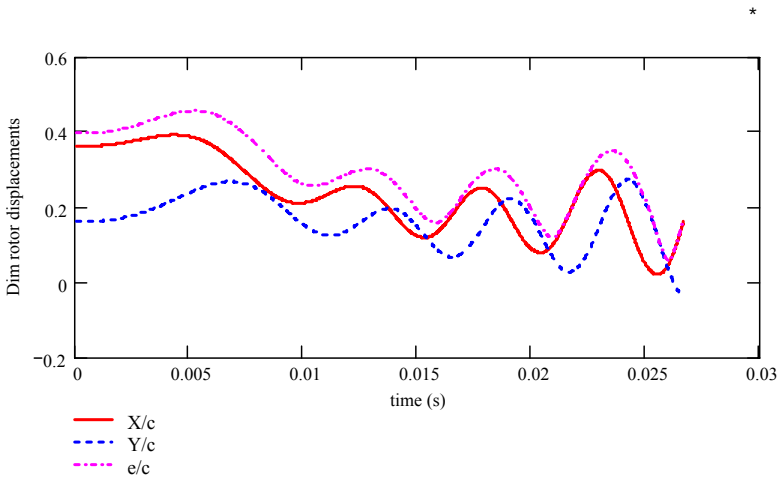

Figure 6b. Predicted dimensionless journal (rotor) eccentricity components versus time. Rotor mass *M*=10 kg

Table 1: Static load and feed pressure and predicted rotor (journal) static position, flow parameters, critical mass and threshold speed of instability

Speed	P Supply	P Exit	Load-X	Load-Y	X/c	Y/c	Mass Flow
rpm	bars	bars	N	N	[-]	[-]	kg/s
5000	5.0	1.0	100	0	0.38	0.15	0.16
10000	6.7	1.0	167	0	0.37	0.23	0.18
15000	11.7	1.0	233	0	0.27	0.18	0.26
20000	20.0	1.0	300	0	0.19	0.14	0.36

Speed	Power Loss	Keq	WFR	Critical mass	10 kg Threshold speed	1 kg Threshold speed
rpm	kW	N/m	-	Kg	rpm	rpm
5000	0.01	3.53E+06	0.50	48.8	11041	34915
10000	0.06	4.80E+06	0.54	12.4	11129	35193
15000	0.17	9.44E+06	0.53	10.8	15576	49255
20000	0.37	1.66E+07	0.53	10.4	20356	64371

Speed	Kxx	Kxy	Kyx	Kyy	Cxx	Cxy	Cyx	Cyy	Mxx	Mxy	Myx	Myy
rpm	N/m	N/m	N/m	N/m	N-s/m	N-s/m	N-s/m	N-s/m	kg	kg	kg	kg
5000	3.59E+06	1.32E+06	-7.54E+05	3.16E+06	3747	484	-621	3783	0.9	-0.2	0.0	1.0
10000	4.13E+06	2.70E+06	-2.67E+06	4.35E+06	4830	1101	-893	4723	0.8	-0.1	0.0	0.8
15000	8.12E+06	5.42E+06	-5.38E+06	8.27E+06	6577	1557	-1448	6494	0.8	-0.1	0.1	0.9
20000	1.43E+07	9.65E+06	-9.53E+06	1.43E+07	8681	2105	-2037	8613	0.9	-0.1	0.1	0.9

Figures 7 and 8 present the applied external load (W_X) and predicted HB reaction force, $|F|$, versus shaft speed and versus time, respectively. For the lowest rotor mass, M=1 kg, inertial effects are negligible; and hence the motion is quasi-static, i.e. for all times, $W_X+F_X=0$ and $F_Y\sim0$. On the other hand, for the large rotor mass, M=10 kg, the bearing reaction force shows a superposition of the static force (W_X) and a periodic force whose magnitude increases steadily as the shaft speed increases. The frequency of the dynamic force component is subsynchronous.

In summary, the numerical predictions obtained for the ramp in shaft speed with varying feed pressure into the hydrostatic bearing and increasing radial loads acting on the rotor are in agreement with prior knowledge. Most importantly, the predictions evidence the importance of rotor mass on the response of the system. That is, for a small rotor mass, "rotor inertia forces" are negligible, and the hydrostatic bearing reacts quasi-statically to the applied external force on the rotor. On the other hand, for a larger rotor mass, the system becomes unstable with a typical ~50% whirl frequency. This phenomenon is predicted accurately from a linear stability analysis of the rotor-bearing system using the bearing force coefficients (stiffness, damping and inertia); albeit the amplitude of motion can only be determined from the solution of the nonlinear equations of motion.

(a) rotor mass, *M*=1 kg

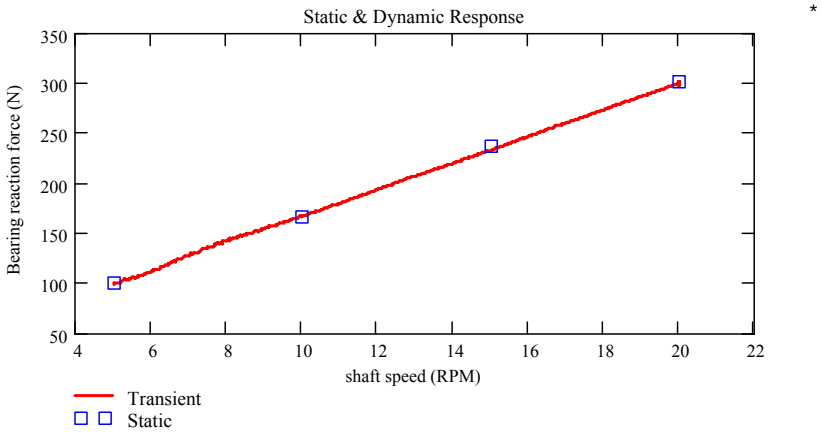

(b) rotor mass, *M*=10 kg

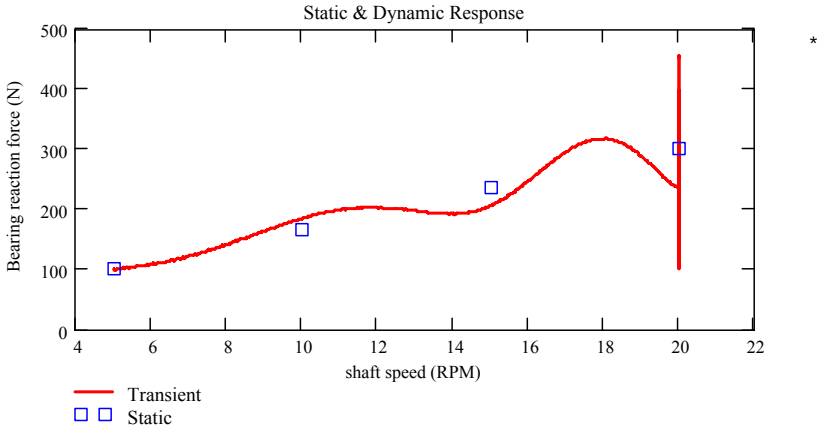

Figure 7: Predicted dynamic and static bearing reaction forces versus shaft speed. (a) M=1 kg, (b) M=10 kg

V. Conclusions

The paper details the unsteady bulk-flow transport equations for prediction of the transient forced response of turbulent flow hydrostatic bearings, the scheme for numerical solution, and including its integration to the dynamic response of a simple rotor-bearing system. The computational bulk-flow model extends earlier analyses and enables the current computational code for ready use in the prediction of transient rotor-speed start ups in cryogenic turbopumps.

Predictions for the transient response of a point mass supported on one water lubricated six-pocket hydrostatic bearing are advanced. A schedule of a fast rotor speed start up is specified along with variations in feed supply pressure into the bearings and increasing static load acting on the rotor. A linear rotordynamic analysis predicts rotor unstable motions with ~50% whirl frequency subsynchronous motions for rotor masses exceeding a critical value. Nonlinear transient rotor response predictions are obtained for two rotor masses, one low and the other nearly equaling the critical magnitude. For the case with largest rotor mass, the predictions evidence the onset of unstable (subsynchronous) whirl motions. On the other hand, the predictions derived for the low rotor mass show a quasi-static dynamic force response with little effect from the rotor accelerations and no unstable motions.

Acknowledgments

The author acknowledges the Air Force Research Laboratory (AFRL), Space & Missile Propulsion Division, Edwards AFB for funding this work. Thanks to Mr. Alan Sutton (AFRL), Mr. Chuck Papesh and Mr. Gordon Dressler (Northrop Grumman) for their interest in the work.

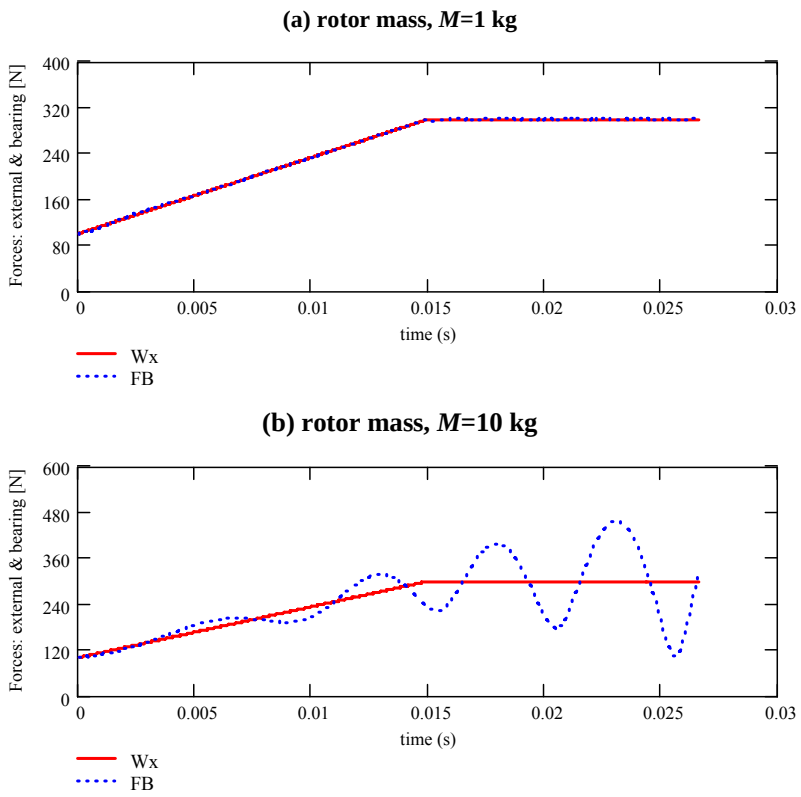

Figure 8: External force and predicted bearing reaction force versus time. (a) M=1 kg, (b) M=10 kg

References

[1]San Andrés, L., "Thermohydrodynamic Analysis of Fluid Film Bearings for Cryogenic Applications", *AIAA Journal of Propulsion and Power,* Vol. 11, No. 5, 1995, pp. 964-972.

[2]San Andrés, L., "Bulk Flow Analysis of Hybrid Thrust Bearings for Process Fluid Applications," *ASME Journal of Tribology*, Vol. 122, No. 1, 2000, pp. 170-180.

[3]Minck, A., and Peery, S., 1998, "Design and Development of an Advanced Liquid Hydrogen Turbopump," AIAA paper No. 98-3681, 34th ASAA/ASME/SAE/ASEE Joint propulsion Conference & Exhibit

[4]San Andrés, L., "Turbulent Hybrid Bearings with Fluid Inertia Effects," *ASME Journal of Tribology*, Vol. 112, 1990, pp. 699-707.

[5]San Andrés, L., "Fluid Compressibility Effects on the Dynamic Response of Hydrostatic Journal Bearings," *WEAR,* Vol. 146, 1991, pp. 269-283.

[6]San Andrés, L., "Analysis of Turbulent Hydrostatic Bearings with a Barotropic Fluid," *ASME Journal of Tribology*, Vol. 114, No. 4, 1992, pp. 755-765.

[7]Yang, Z., San Andrés, L., and Childs, D., "Thermohydrodynamic Analysis of Process Liquid Hydrostatic Bearings in Turbulent Regime, I: The Model and Perturbation Analysis, II: Numerical Solution and Results", *ASME Journal of Applied Mechanics,* Vol. 62, No. 3, 1995, pp. 674-684.

[8]San Andrés, L., "Turbulent Flow, Flexure-Pivot Hybrid Bearings for Cryogenic Applications," *ASME Journal of Tribology*, Vol. 118, 1, 1996, pp. 190-200.

[9]Kurtin, K., Childs, D., San Andrés, L., and Hale, K., "Experimental versus Theoretical Characteristics of a High Speed Hybrid (combination Hydrostatic and Hydrodynamic) Bearing", *ASME Journal of Tribology*., Vol. 115, No. 1, 1993,pp. 160-169.

[10]Franchek, N., Childs, D., and San Andrés, L., "Theoretical and Experimental Comparisons for Rotordynamic Coefficients of a High-Speed, High-Pressure, Orifice-Compensated Hybrid Bearings," *ASME Journal of Tribology*, Vol. 117, No. 2, 1995, pp. 285-290.

[11]San Andrés, L., and Childs, D., "Angled Injection - Hydrostatic Bearings, Analysis and Comparison to Test Results," *ASME Journal of Tribology*, Vol. 119, No. 1, 1997, pp. 179-187.

[12]San Andrés, L., "A Hybrid Bearing with Improved Rotordynamic Stability," 1st International Conference in Rotordynamics of Machnery [CD-ROM], ISCORMA1, Lake Tahoe (NV), 2001, Paper No. 2006.

[13]San Andrés, L., "Annular Pressure Seals and Hydrostatic Bearings," RTO-AVT-VKI Lecture Series 2006, Design & Analysis of High Speed Pumps, March 20-23, Publication No. RTO-MP-AVT-143, Von Karman Institute for Fluid Mechanics, Belgium, 2006.
[14]San Andrés, L., "Transient Response of Externally Pressurized Fluid Film Bearings," *STLE Tribology Transactions*, Vol. 40, No. 1, 1997, pp. 147-155.
[15]Hirs, G.G., "A Bulk-Flow Theory for Turbulence in Lubricant Films, *ASME Journal of Lubrication Technology,* Vol. 94, 1973, pp. 137-146.
[16]Launder, B.E., and M. Leschziner, "Flow in Finite Width Thrust Bearings Including Inertial Effects, I-Laminar Flow, II-Turbulent Flow," *ASME Journal of Lubrication Technology,* Vol. 100, 1978, pp. 330-345.
[17]Van Doormaal, J. P., and Raithby, G. D., "Enhancements of the SIMPLE Method for Predicting Incompressible Fluid Flows," *Numerical Heat Transfer,* Vol. 7, 1984, pp. 147-163.
[18]San Andrés, L., 2002, "Numerical Evaluation of Unsteady Bulk-Flow in Fluid Film Bearings," Modern Lubrication Theory, Notes No. 10, Texas A&M University, http://phn.tamu.edu/me626 (accessed January, 2006)
[19]Bathe, K., Finite Element Procedures in Engineering Analysis, Prentice-Hall, Englewood Cliffs, NJ, 1982, pp. 508-511.

Start-up Response of Fluid Film Lubricated Cryogenic Turbopumps

Luis San Andres
Mechanical Engineering Department
Texas A&M University
College Station, TX 77843-3123

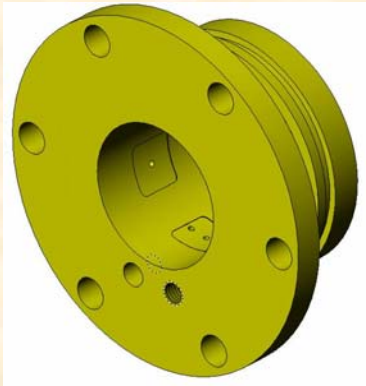

Work supported by AFRL

AIAA 2007-5093

Hydrostatic bearings for turbopumps

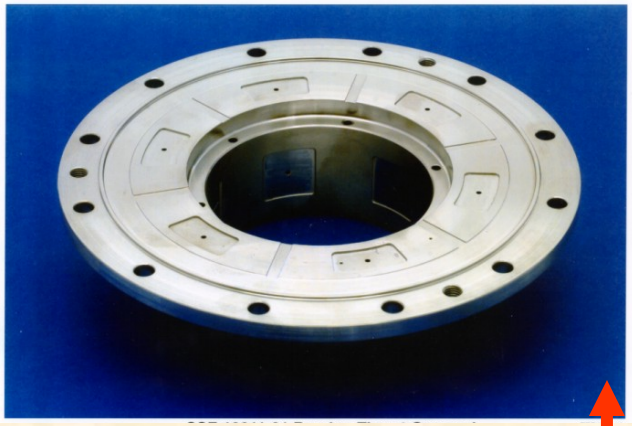

Thrust hydrostatic bearing

Low cost primary power cryogenic turbo-pumps (TP) are compact, operate at high speeds, and require of externally pressurized fluid film bearings to support radial and thrust loads.

Radial hydrostatic Bearing

Hybrid thrust & radial bearings enable smaller and lighter turbopumps with no DN life limitations

Large stiffness (accuracy of positioning) and damping force coefficients allow for unshrouded impellers with increased TP efficiency

Justification

Approved for Public Release, distribution unlimited.

Hydrostatic Bearings for Cryogenic Turbo Pumps

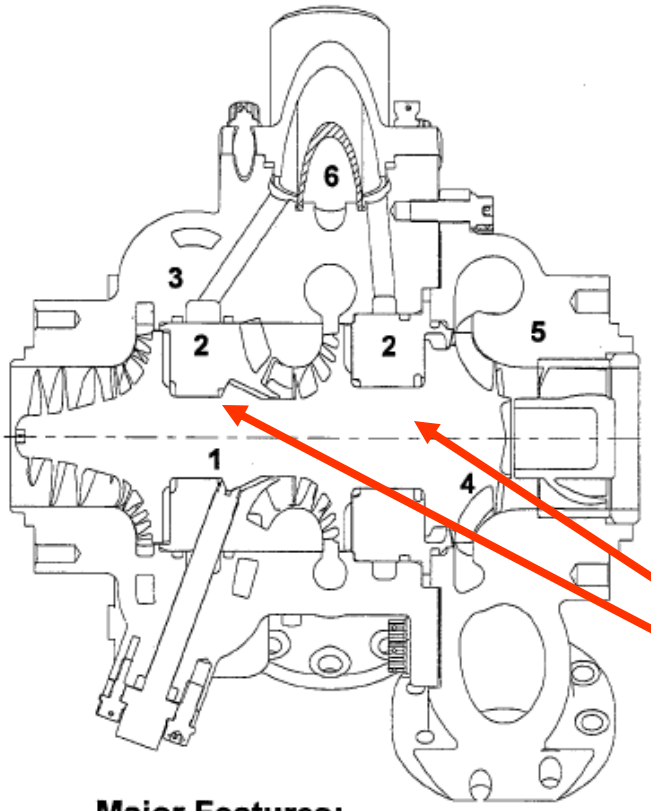

Major Features:

1 One piece titanium rotor.
2 Split hydrostatic bearings.
3 Cast pump housing with integral crossover passages.
4 Radial inflow turbine.
5 Cast turbine housing with vaneless inlet volute.
6 Filtered bearing supply.

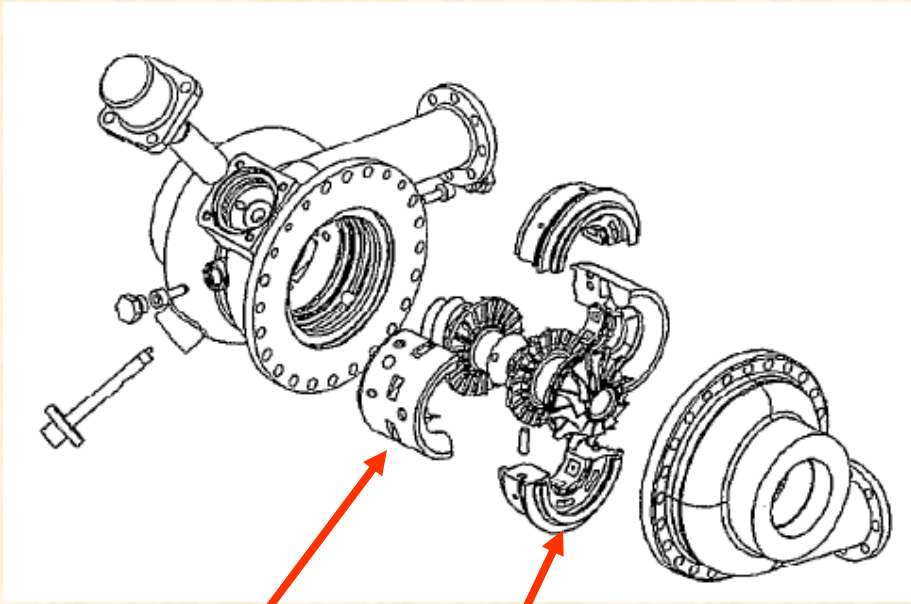

Radial hydrostatic bearings

Thrust hydrostatic bearing

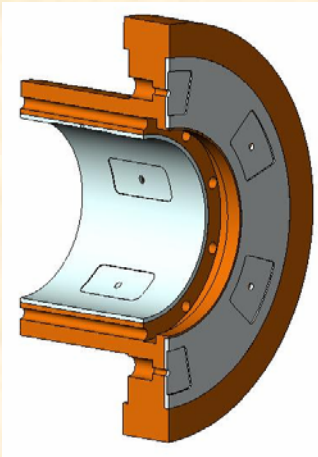

Minck, A., and Peery, S., 1998, "Design and Development of an Advanced Liquid Hydrogen Turbopump," AIAA paper No. 98-3681, 34th ASAA/ASME/SAE/ASEE Joint propulsion Conference & Exhibit

Advanced Liquid Hydrogen Turbopump

Hydrostatic Bearings for pump applications

External pressure source forces fluid to flow between two surfaces, thus enabling their separation and the ability to support a load without contact.

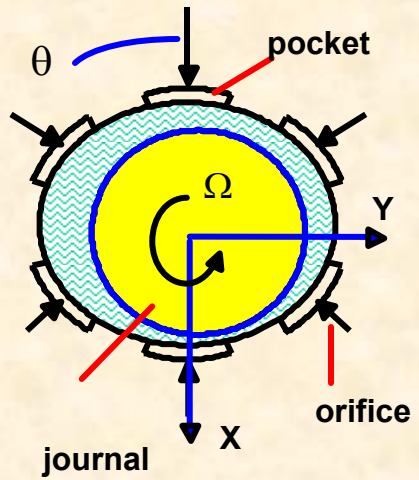

Support very large loads. The load support is a function of the pressure drop across the bearing and the area of fluid pressure action.

Load does not depend on film thickness or lubricant viscosity

Long life (infinite in theory) without wear of surfaces

Provide stiffness and damping coefficients of very large magnitude. Excellent for exact positioning and control.

Advantages of Hydrostatic Bearings

Hydrostatic Bearings for pump applications

Require ancillary equipment. Larger installation and maintenance costs.

Need of fluid filtration equipment. Loss of performance with fluid contamination.

High power consumption: pumping losses.

Limited LOAD CAPACITY ~ f(P_{supply})

Potential to induce hydrodynamic instability in hybrid mode operation (with rotor spinning).

Potential to show pneumatic hammer instability with compressible fluids

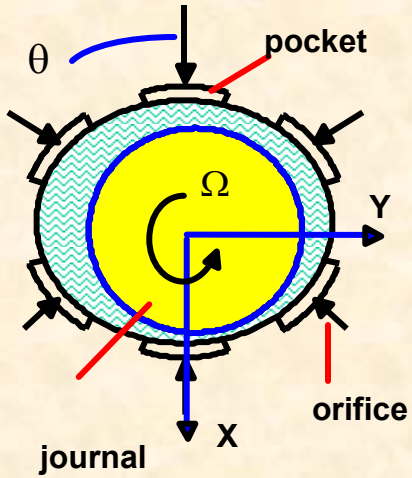

Disadvantages of Hydrostatic Bearings

Conventional hydrostatic bearing design

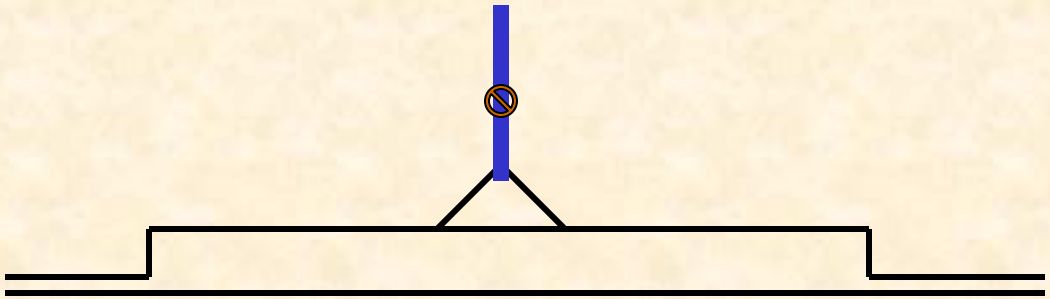

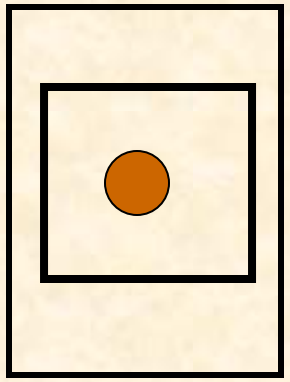

* large pocket area (80-90 % of total area)
* deep pocket depth (>>> clearance)
* large orifice discharge volume

Applications:

low or null surface speed, low frequencies,
nearly **incompressible** fluids (water or mineral oil)
produces very large DIRECT Stiffness.

Warning: **This design should NOT be used with compressible liquids or gases**

Hydrostatic Bearings for Cryogenic Turbo Pumps

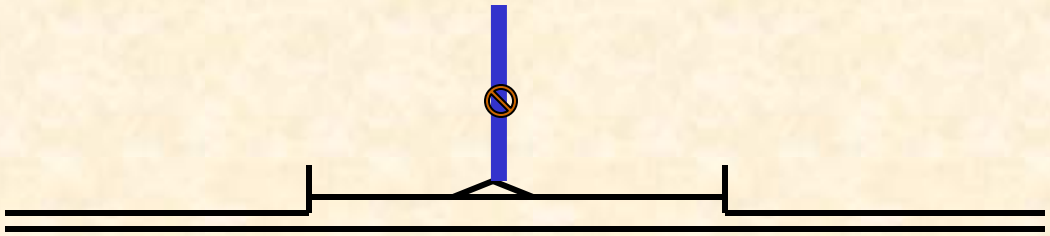

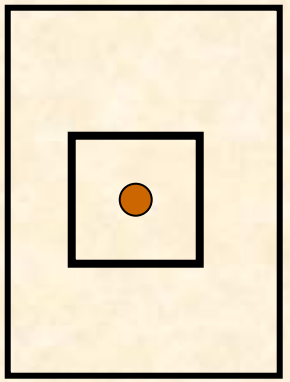

* small pocket area (10%-25 % of total area)
* shallow pocket depth
* small or null orifice discharge volume

Nearly inherent restrictor type, i.e. orifice coefficient regulated by clearance

Applications:

high surface speeds, low and high frequencies, **compressible** liquids (LO_2, LH_2, LN_2)

+ Angled injection against rotation to reduce cross-coupled stiffnesses (avoid hydrodynamic instability)

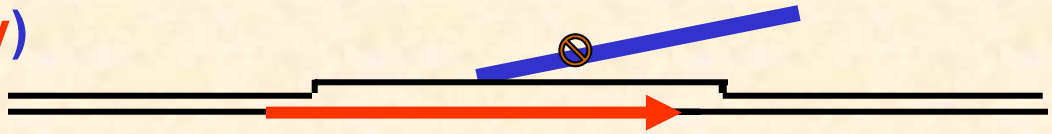

Cryogenic fluid hydrostatic bearing design

Past Work at TAMU

HYDROJET® – bearing model (1990-1996)

hydrostatic/hydrodynamic radial bearings,
angled injection, roughened surfaces

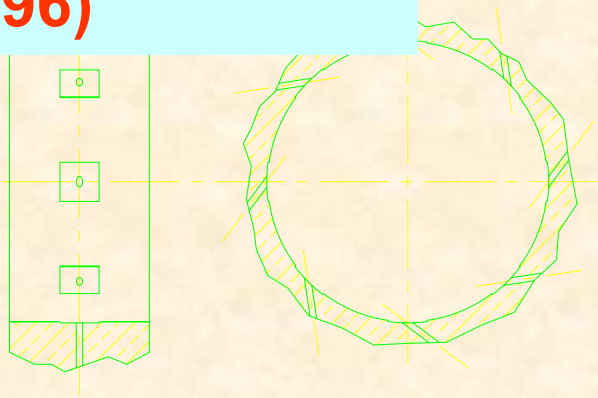

Honeycomb seals and annular damper seals

tilting and flexure pivot journal bearings,
simple foil bearings,

HYDROTHRUST® – bearing model (1998-2000)

hydrostatic/hydrodynamic thrust bearings

inner pressurized face seals with angular misalignment

Bulk-Flow Codes include full fluid inertia, turbulence flow and thermohydrodynamic models for high-speed, high-pressure, hot/cold cryogenic and process fluid operating conditions.
Cryogenic fluids: LO_2, LH_2, LN_2 & Methane

Past Work at TAMU (Childs et al.)

HYDROJET® – radial hydrostatic bearings

Tests with water (1000 psi max, 25 krpm max).
+ 20 bearings x 3 clearances & 2 pocket depths, different pocket shapes, macro-roughness (surface textured) bearings, angled injection.
Water Lomakin Bearings

Gas Honeycomb seals
Mineral Oil tilting and flexure pivot journal bearings

HYDROTHRUST ®– axial thrust hydrostatic bearings

NONE available in literature for high speed, high pressure (turbulent flows). Tests planned for Su 2007

Validation (benchmarking) of bulk-flow codes

Past Work at TAMU (Childs et al.)

Physical variable - prediction	Experimental validation (+/- Accuracy %)	Notes
Bearing flow rate & pocket pressures	**YES (2 %)**	Empirical orifice coefficient extracted
Drag torque & power and temperature raise	**YES (2 %)**	Must not reduce TP efficiency. Cryogen cannot exit too hot (vaporization)
load capacity (fluid film forces and restoring moments),	**YES (5 %)**	Radial Load – Linear with journal displacement
16 complex impedance force coefficients due to dynamic journal center displacements and journal axis rotations	**YES (5 %, 20%) (10 %) (30 %)**	Lateral (radial) motions only stiffness: K_{XX}, K_{YY} , K_{XY}, K_{YX}, damping: C_{XX}, $C_{YY,}$ C_{XY}, C_{YX}, inertia: M_{XX}, $M_{YY,}$ M_{XY}, M_{YX},
Whirl frequency ratio for lateral shaft motions	**YES (10 %)**	**WFR ~ 0.50** for smooth surface bearing and radial fluid injection
Warning for pneumatic hammer instability	**YES**	Tests with water-GN_2

Test Validation of Radial Hydrostatic Bearing Predictions

Objective

Prediction of Start-up response of an all-fluid film bearing cryogenic TP by

creating capability for modeling **non-linear forced response of fluid film radial bearing**, i.e. bearing reaction forces (impedance models) as a function of instantaneous journal position, velocity and acceleration

Procedure: Solution of unsteady bulk-flow equations in fluid film bearing and integration to (nonlinear) rotordynamics model for prediction of rotor-bearing transient response.

Unsteady bulk-flow equations in film lands

- Turbulent flow with fluid inertia effects
- Mean flow velocities – average across film (h)
- Not valid in flow zones with strong recirculation

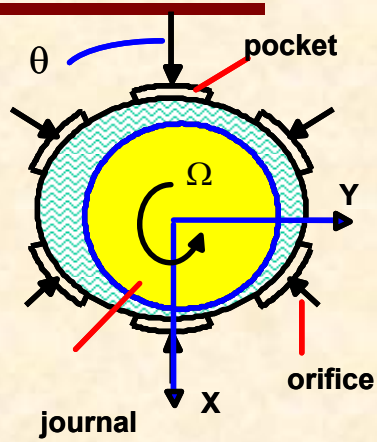

Continuity:

$$\frac{\partial(\rho h)}{\partial t}+\frac{\partial(\rho H U_z)}{\partial z}+\frac{1}{R}\frac{\partial(\rho H U_\theta)}{\partial\theta}=0$$

Axial momentum

$$\frac{\partial(\rho H U_z)}{\partial t}+\frac{\partial(\rho H U_z^2)}{\partial z}+\frac{1}{R}\frac{\partial(\rho H U_z U_\theta)}{\partial\theta}=-H\frac{\partial P}{\partial z}-\frac{\mu}{H}(\kappa_z U_z)$$

Circumferential momentum

$$\frac{\partial(\rho H U_\theta)}{\partial t}+\frac{\partial(\rho H U_z U_\theta)}{\partial z}+\frac{1}{R}\frac{\partial(\rho H U_\theta^2)}{\partial\theta}=-\frac{H}{R}\frac{\partial P}{\partial\theta}-\frac{\mu}{H}\left(\kappa_\theta U_\theta-\kappa_J\frac{\Omega R}{2}\right)$$

Thermal transport

$$C_p\left\{\frac{\partial(\rho HT)}{\partial t}+\frac{\partial(\rho H U_z T)}{\partial z}+\frac{1}{R}\frac{\partial(\rho H U_\theta T)}{\partial\theta}\right\}=-Q_{BS}+\beta_T H T\left(\frac{\partial P}{\partial t}+U_z\frac{\partial P}{\partial z}+\frac{1}{R}U_\theta\frac{\partial P}{\partial\theta}\right)+R\Omega\cdot\tau_{y\theta}\Big|^h+U_z\cdot\Delta\tau_{zy}+U_\theta\cdot\Delta\tau_{y\theta}$$

$$Q_{BS}=Q_B+Q_S=h_B(T-T_B)+h_S(T-T_S)$$

Unsteady Bulk Flow Equations in Pockets

Pocket pressure field with angled injection

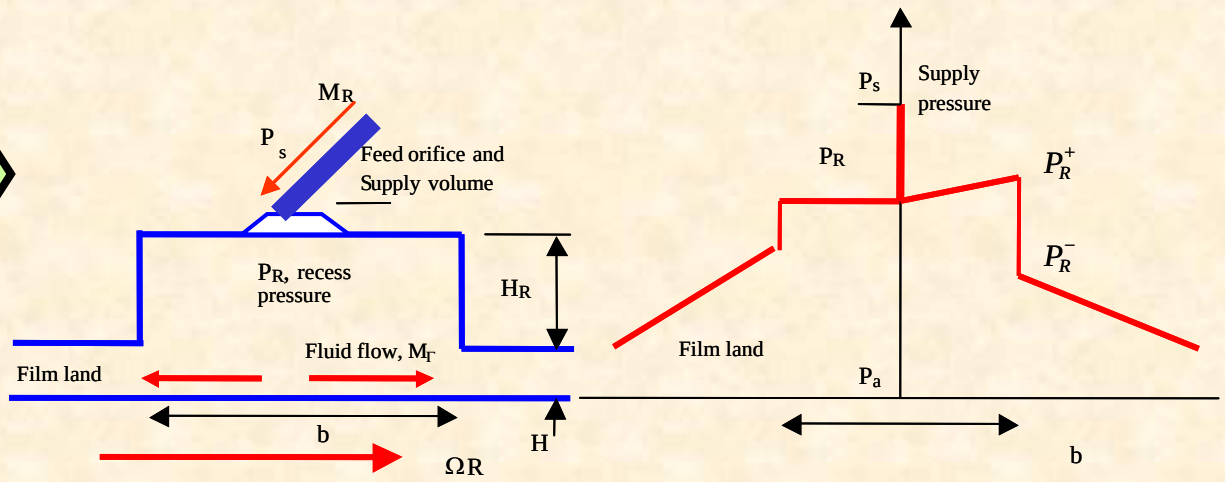

Flow continuity

$$M_R = C_d\, A_o \left(\frac{\rho}{2}\left[P_s - P_R\right]\right)^{1/2} = M_\Gamma + \frac{\partial}{\partial t}\left(\rho V_R\right)$$

Pressure rise before edge

$$P_R^+ = P_R + \mu\kappa_x \frac{b}{2\left(h+h_R\right)^2}\left\{\frac{\Omega R}{2} - V_x\right\}_R$$

Pressure rise at edge

$$P_R^- = P_R^+ + \frac{(1+\xi)}{2}\rho\left[1 - \left(\frac{\rho_e^-}{\rho_e^+}\right)\left(\frac{h}{h+h_R}\right)^2\right]V_{x,z}^2$$

Pocket pressures: angled & radial injection

Find bearing reaction forces (F_X,F_Y) as a function of rotor position and velocity.

Other quantities of interest are: flow rate, drag torque, power loss, fluid temperature rise. Implements perturbation of unsteady flow field to calculate (stiffness, damping and inertia) force coefficients

$$Z_{\alpha\beta} = -\oint_{A_B} \{P_\beta H_\alpha\} R\, dz\, d\theta = K_{\alpha\beta} - \omega^2 M_{\alpha\beta} + i\,\omega C_{\alpha\beta}\,; \quad \alpha,\beta = X,Y$$

Numerical method of solution:

Fluid Flow: SIMPLEC control-volume method, implicit time response scheme with local linearization

Rotordynamics: Integration into in-house rotordynamics program (FE-component mode synthesis)

Results & Numerical Analysis Methods

Example: start up water HB test rig

Fluid: warm water at 50°C

Max rotor speed = 20 krpm,

Max water feed pressure = 20 bar

Applied loads =

Fn. of rotor speed

Pocket depth/*c* ~ 7
Pocket area ~ 20 %
to avoid water hammer

Emulates typical start-up conditions in a cryogenic turbopump

Bearing Loads FROM PUMP Start Up

Pressure supply ~ RPM² (bleed off from pump discharge)

Predict transient response

Geometry and operating conditions for water HB rig

Rotor-Bearing System EOMS

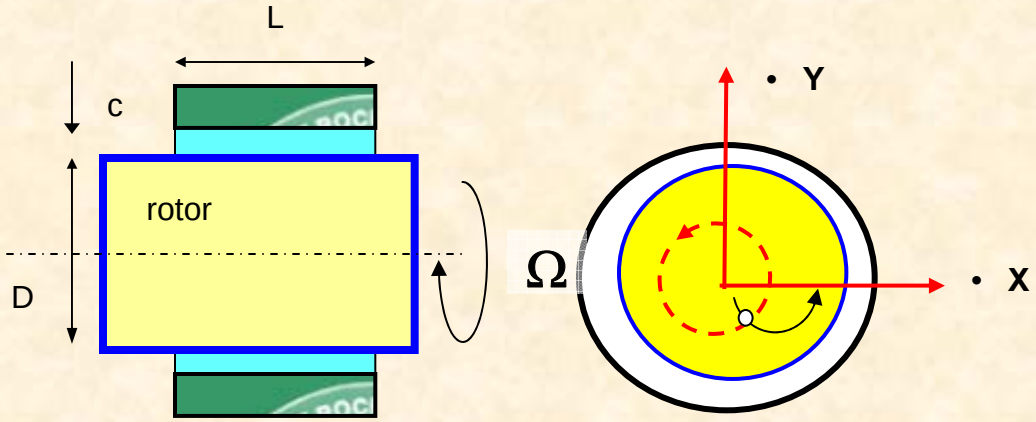

Numerical integration of

M ax = Wx+Fx, M ay= Wy+Fy

where

ax=d(vx)/dt, **ay** = d(vy)/dt : accelerations

vx = d**X**/dt, **vy** = d**Y**/dt: velocities

M: point mass (rigid) rotor

Wx, Wy: external loads including weight

Fx,Fy: bearing reaction loads

Investigate effect of rotor mass on transient response and stability of rotor-bearing system

Example: Start up of Water Test Rig

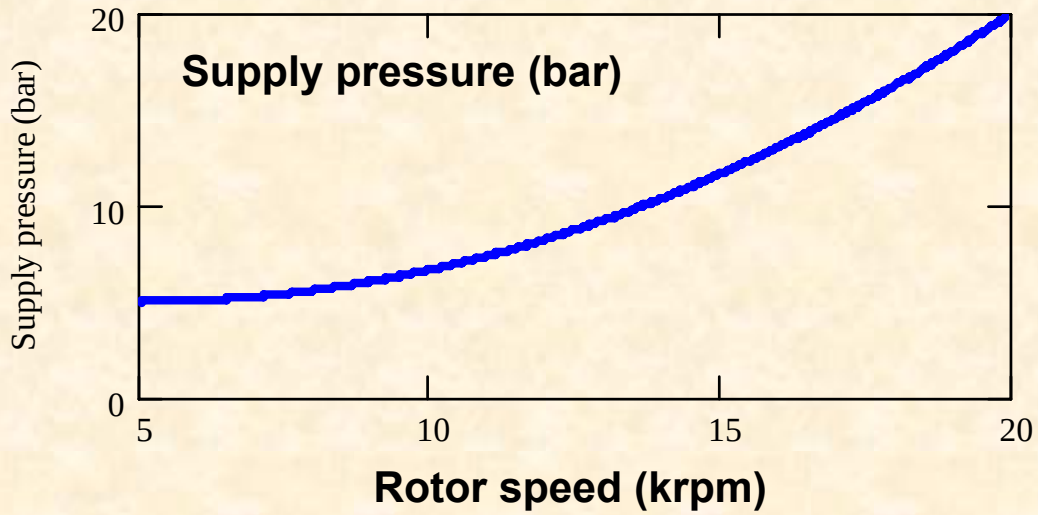

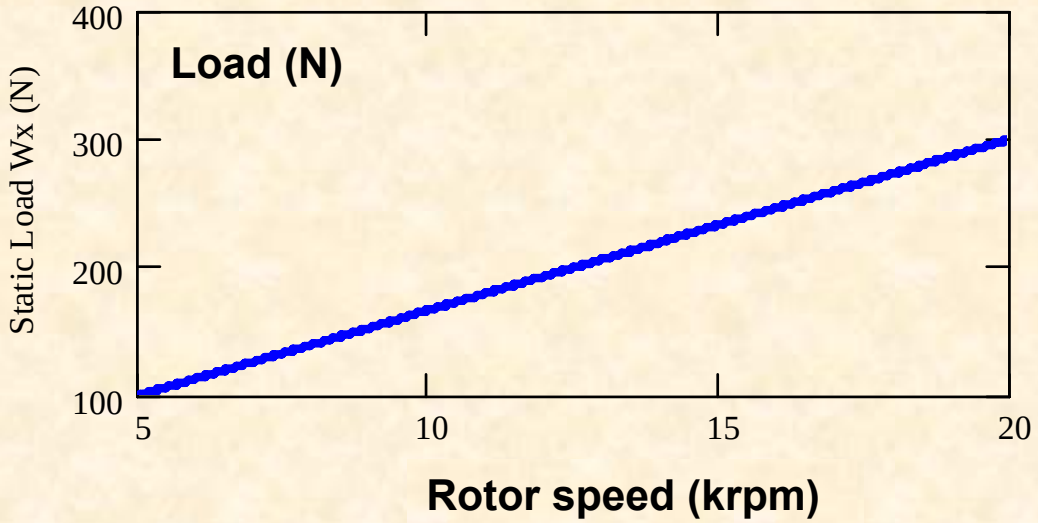

Feed pressure into bearings and external loads on rotor tied to rotor speed

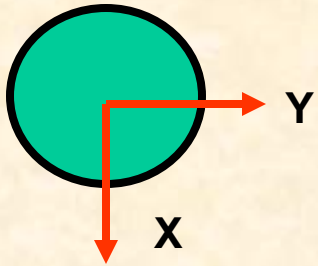

Supply pressure and static load vs. rotor speed

Example: Start up of Water Test Rig

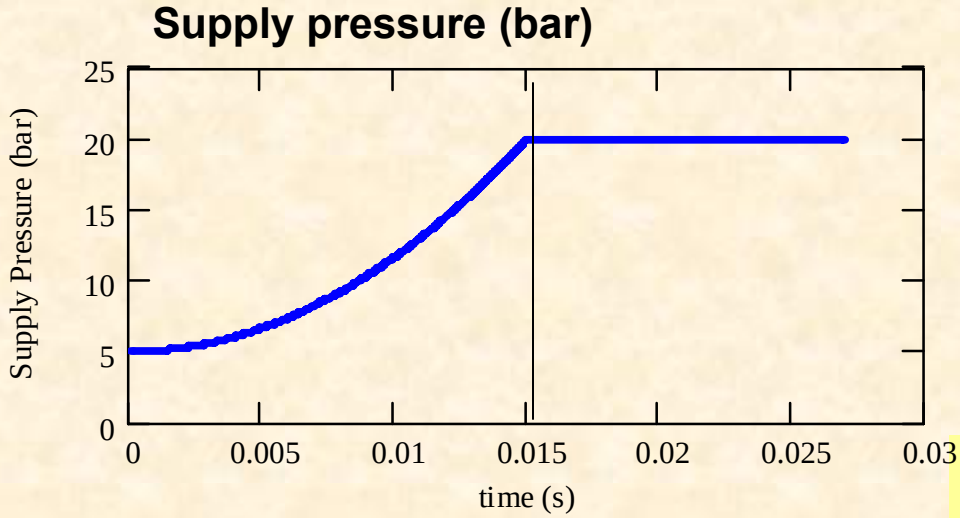

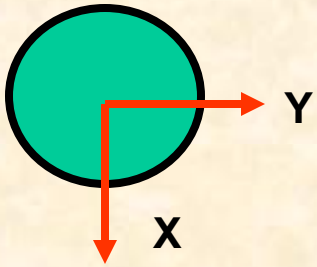

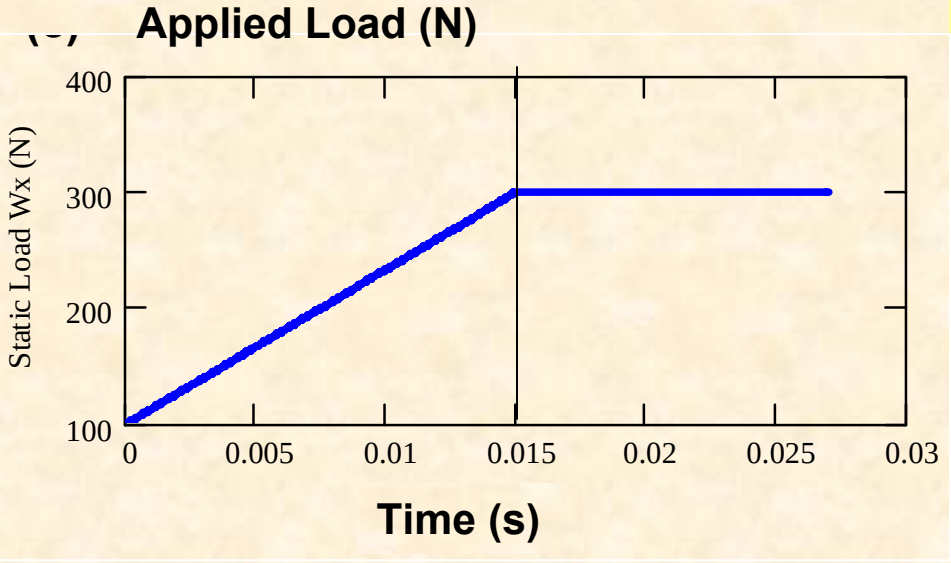

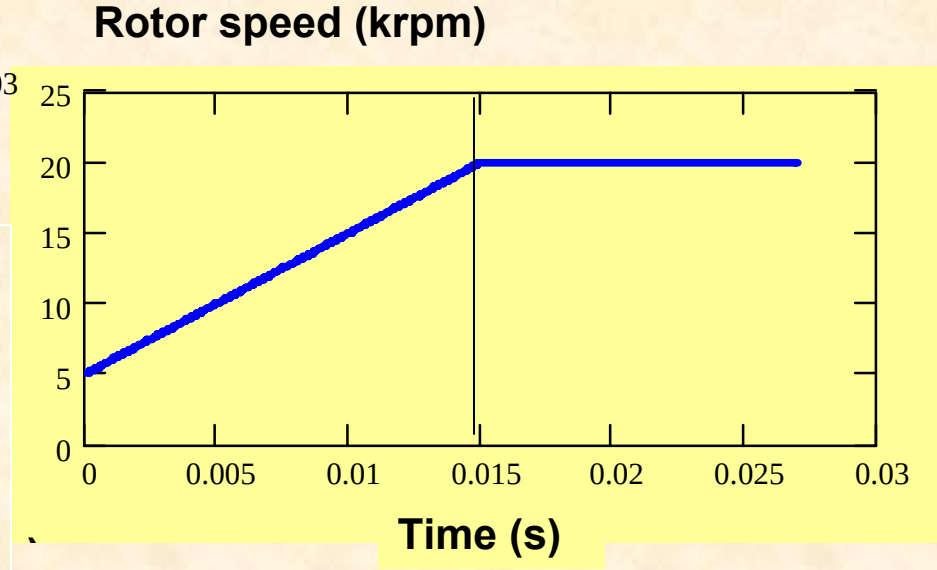

Rotor speed, supply pressure and static load vs. time for water HB

Example: Start up of Water Test Rig

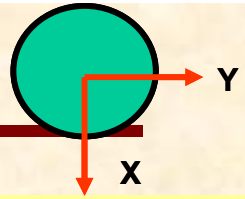

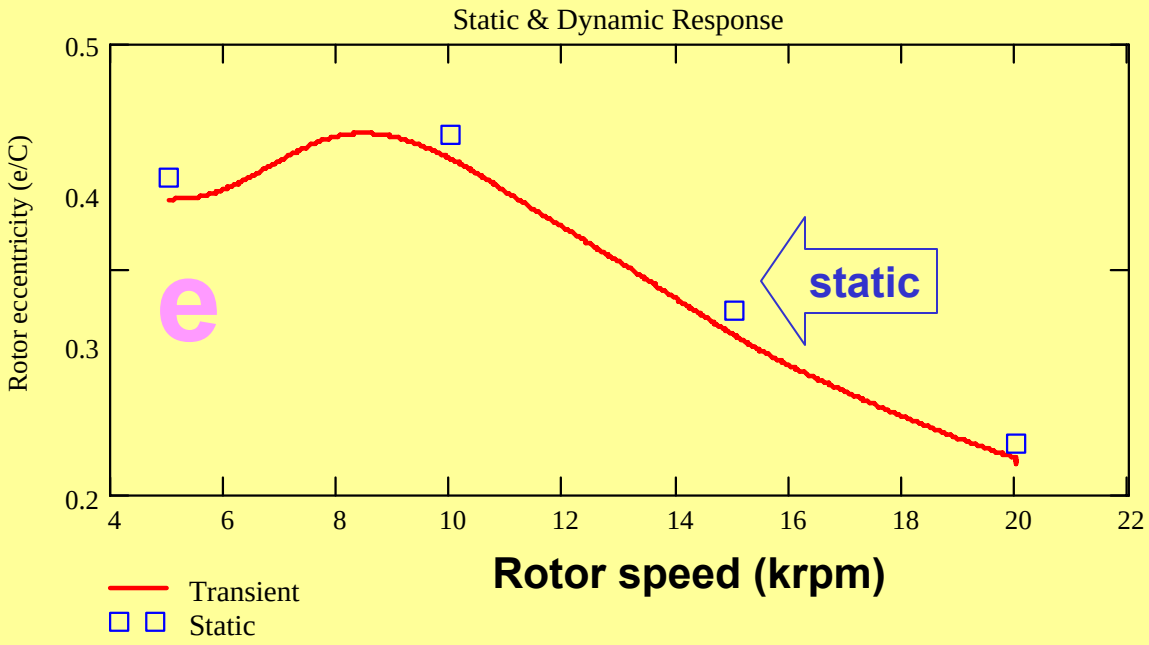

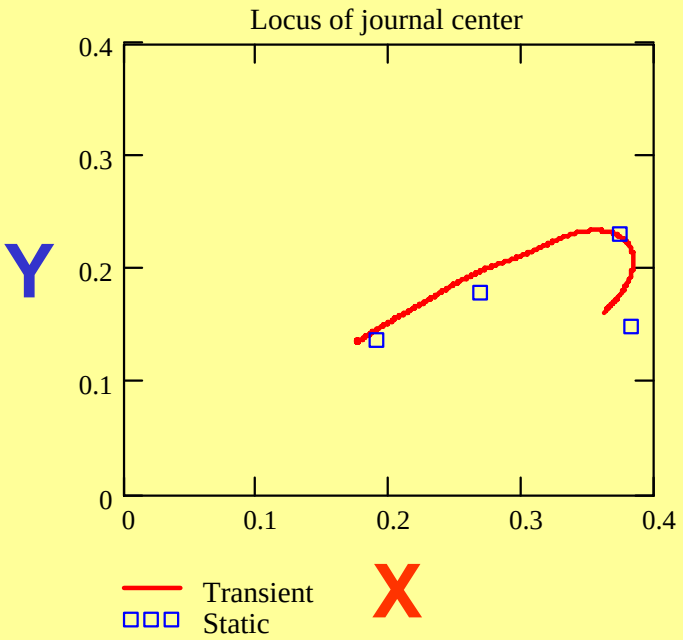

For low rotor mass: smooth and stable transient response, rotor reaches steady state condition. Quasi-static analysis is sufficiently accurate for prediction of response

Transient rotor position (eccentricity) vs. shaft speed, M= 1 kg

Example: Start up of Water Test Rig

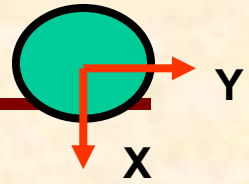

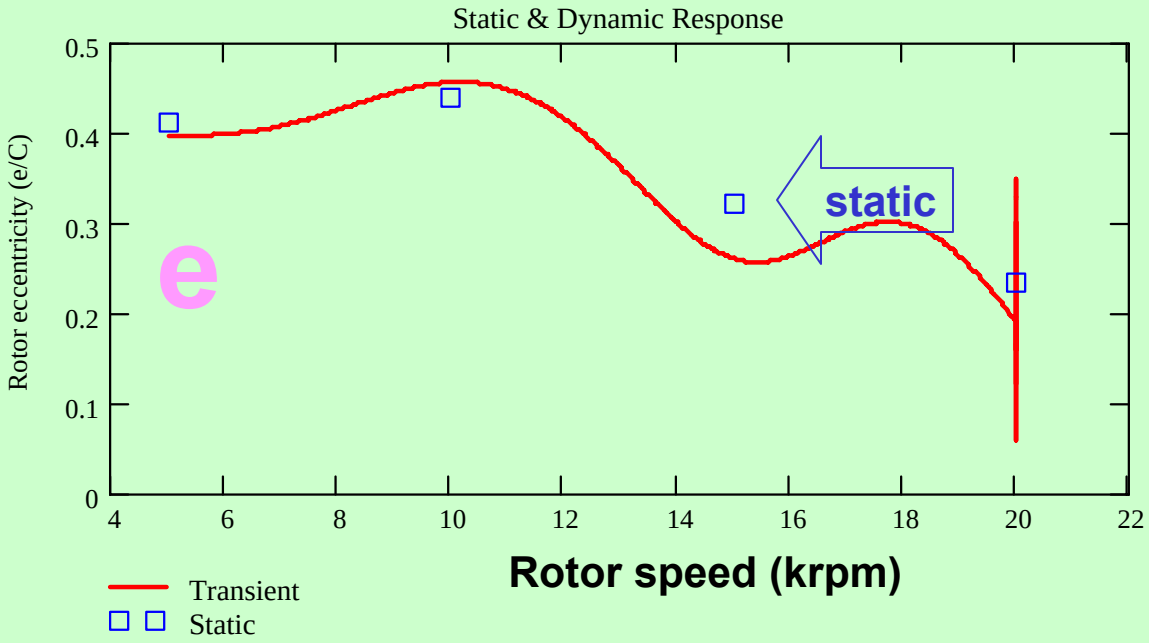

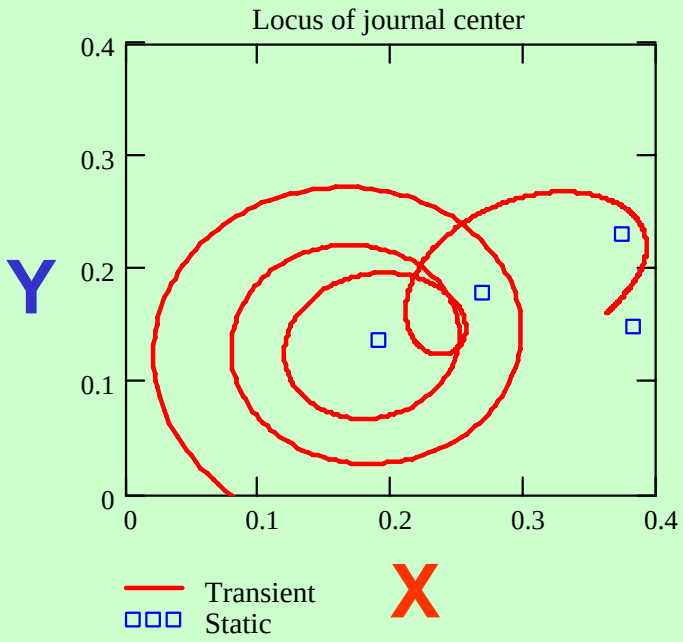

For high rotor mass: smooth and stable transient response, but rotor begins to whirl at max speed. Quasi-static analysis is NOT accurate for prediction of system response

Transient rotor position (eccentricity) vs. shaft speed, M= 10 kg

Example: Start up of Water Test Rig

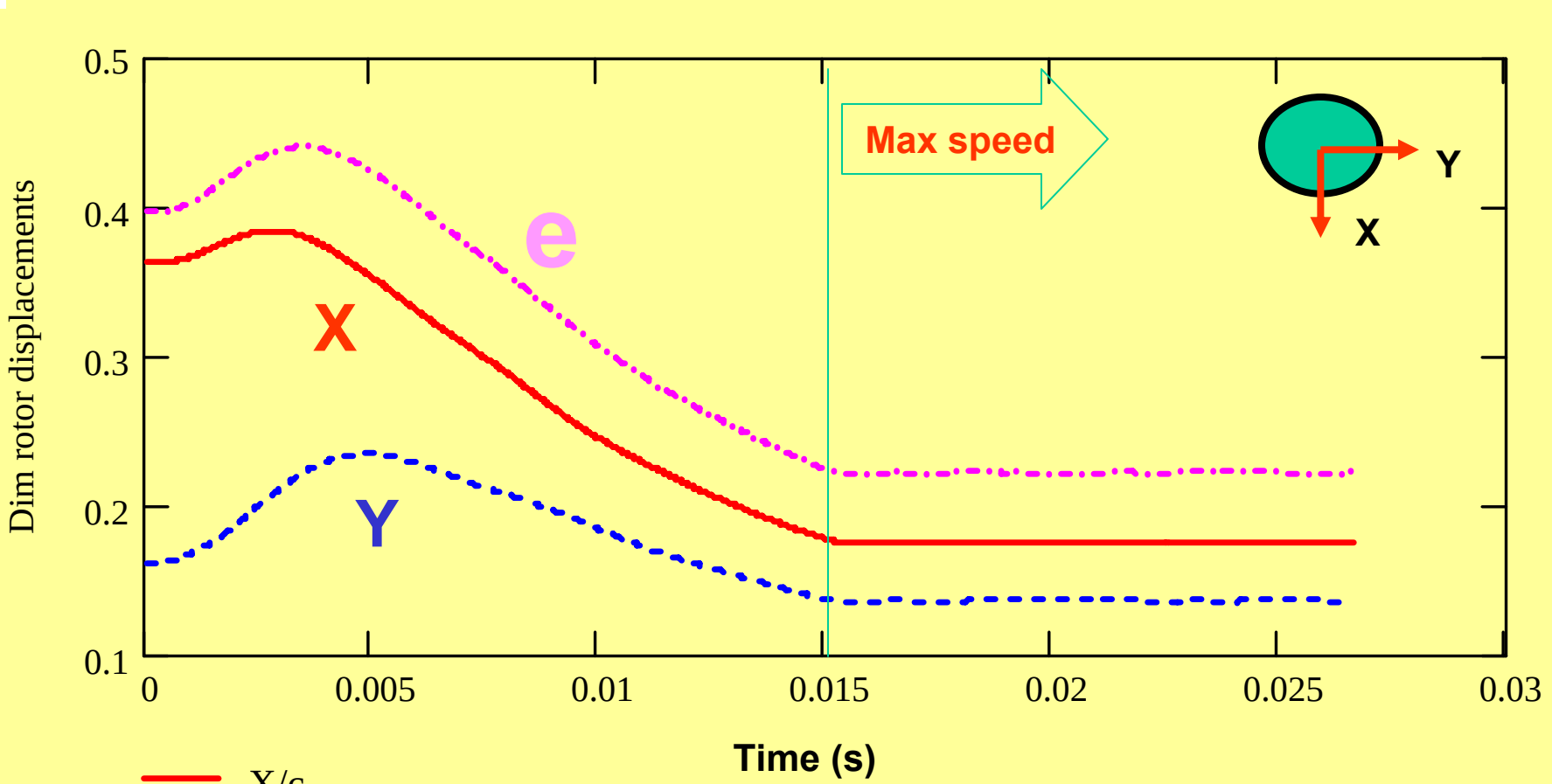

For low rotor mass: smooth and stable transient response, rotor reaches steady state condition.

Transient rotor position (eccentricity) vs. time, M= 1 kg

Example: Start up of Water Test Rig

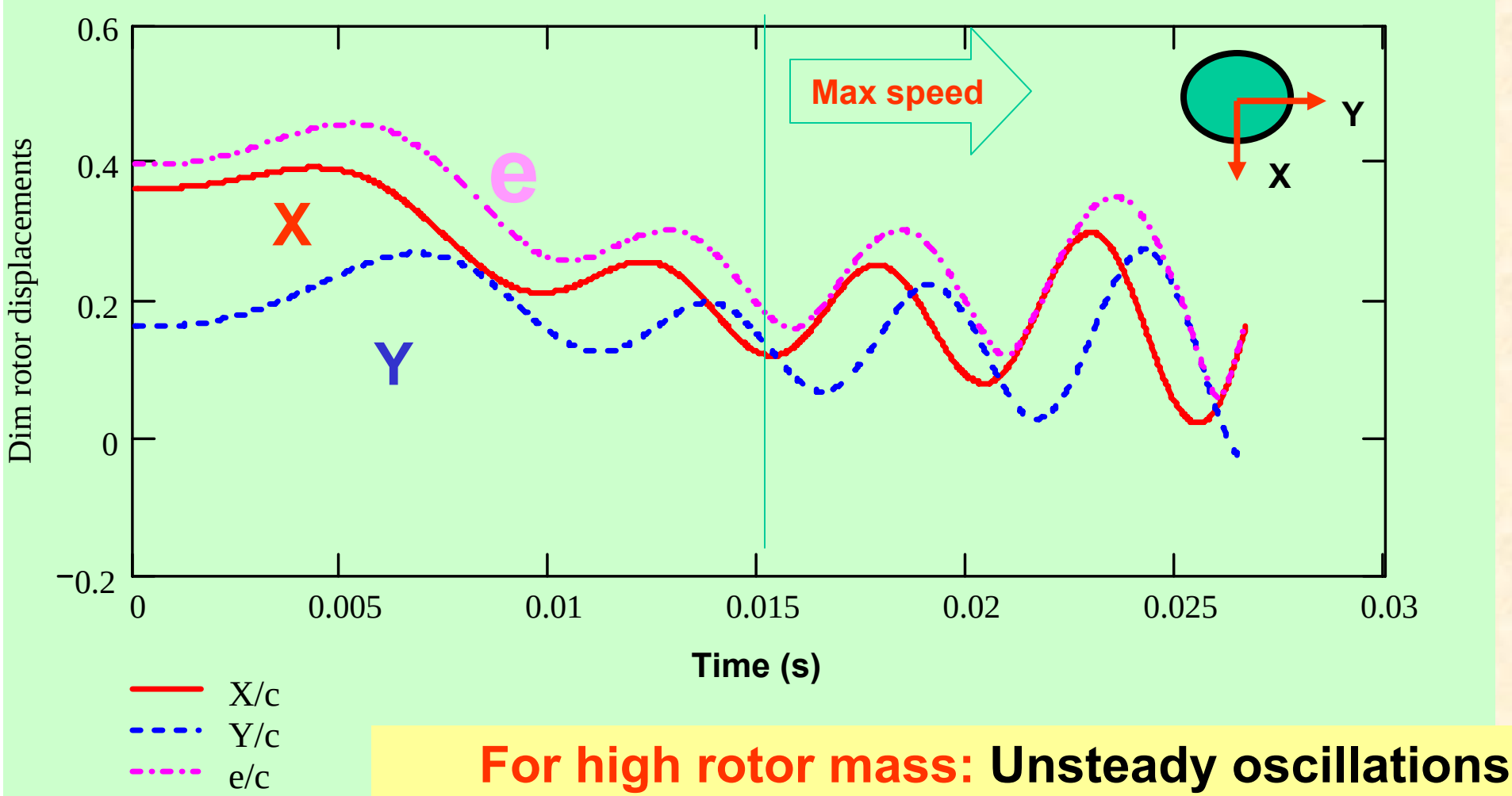

For high rotor mass: Unsteady oscillations lead to rotordynamic instability at max speed

Transient rotor position (eccentricity) vs. time, M= 10 kg

Conclusions

Predictions for the start-up response of a rigid rotor supported on one water lubricated hydrostatic bearing. Schedule of rotor speed start up specified along with changes in supply pressure into the bearing and increasing static load acting on rotor.

Linear rotordynamic analysis predicts rotor unstable motions with ~50% whirl frequency subsynchronous motions for rotor masses exceeding a critical value.

Nonlinear transient rotor response predictions obtained for two rotor masses, one low and the other nearly equaling the critical magnitude.

For largest rotor mass, predictions verify onset & persistence of unstable (subsynchronous) whirl motions.

Predictions for low rotor mass show a quasi-static forced response with little effect from rotor accelerations and showing no unstable motions

Hydrostatic Bearings – Recommendations

HBs have WFR > ~ 0.50 limiting their application to ~2x critical speed. Limiting speed condition can be LOWER if fluid is compressible and pockets are too deep & of large area. To reduce risk of hydrodynamic instability & to increase bearing stability margin:

-Texture bearing surface

Proven with macro "rough" surfaces such as
Knurled, round hole and tire truck pattern tested successfully

-Angled injection against rotation

Retards circumferential flow swirl, effectiveness reduces at high rotor speeds, Can induce backward whirl. Tested successfully

-Introduce bearing asymmetry

Geometrically build stiffness orthotropy ($K_{XX} > K_{YY}$)
Axial feed grooves, mechanical preload, etc. Tested & patented!

Hydrostatic Bearings – Learn more

Learn more:

http://phn.tamu.edu/TRIBGroup

http://phn.tamu.edu/me626

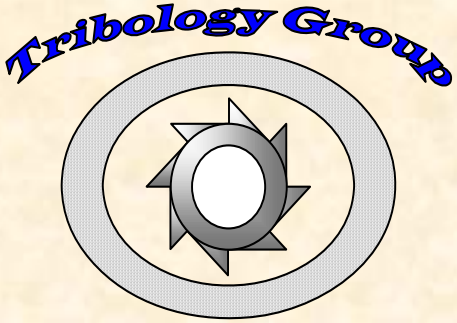

Thanks to AFRL & Northrop Grumman for interest & financial support